International Journal of Heat and Mass Transfer 165 (2021) 120677

Contents lists available at ScienceDirect

International Journal of Heat and Mass Transfer

journal homepage: www.elsevier.com/locate/hmt

Dynamic characteristics of solid packed-bed thermocline tank using molten-salt as a heat transfer fluid

ELSaeed Saad ELSihy[a], Zhirong Liao[a], Chao Xu[a], Xiaoze Du[a,b,*]

[a] Key Laboratory of Condition Monitoring and Control for Power Plant Equipment (North China Electric Power University) Ministry of Education, Beijing, 102206, PR China

[b] School of Energy and Power Engineering, Lanzhou University of Technology, Lanzhou 730050, China

ARTICLE INFO

Article history:
Received 18 August 2020
Revised 14 October 2020
Accepted 1 November 2020
Available online 13 November 2020

Keywords:
thermal energy storage
thermocline
packed-bed
local non-equilibrium thermal theory
discharge power

ABSTRACT

Thermocline characteristics and the discharge performance of a molten-salt packed-bed energy storage system are analyzed numerically. For this purpose, a transient two-dimensional model based on local non-equilibrium thermal theory in a porous medium is developed. Three different solid fillers are utilized, including that of quartzite rock, slag pebbles, and alumina ceramics. Molten-salt serves as a heat transfer fluid (HTF). The effects of fluid inlet flow rate and the particle size diameter on the thermocline thickness through temperature profiles of packed-bed systems have been investigated. The discharging power is discussed in a detailed description of various operating conditions through the discharge outlet temperature stability period. The results obtained are compared with that of the pure molten-salt tank. It is revealed that the thermocline thickness of the molten-salt packed-bed tank is higher than that of pure molten-salt tank, while the latter is better in thermal stratification. As the inlet flow rate increases, both the discharging power and thermocline thickness increase. The results also indicated that decreasing particle size diameter, results in a decrease in thermocline thickness, and the discharging performance becomes more stable. Slag pebbles as a filler material is more effective than quartzite rock in thermal energy storage (TES). The results can be beneficial for the design and optimization of the packed-bed thermocline tank.

1. Introduction

Ensuring compliance with the stringent environmental regulations have dictated to reduce the amount of conventional fossil fuels with harmful effects, as well as the search for renewable energy resources, including that of solar and wind power. With respect to solar power, the incoming solar radiation to the earth's surface is about 51% of the total radiation reaches the upper atmosphere [1]. This enormous, free, and non-polluting energy needs to be utilized efficiently to compensate the gap between the increasing demand and the continuous shortage of the limited supply of the conventional energy resources [2,3].

Among the solar applications systems, concentrated solar power (CSP) has higher efficiency and is the most commercially used technology. Besides, the concentrated solar power (CSP) station integrated with thermal energy storage (TES) has been proved to be an ideal peak regulation approach to the intermittency and uncertainty of solar energy, which has presented a significant challenge to their power output and affected the stability of the grid, as well as lead to severe power curtailment [4,5]. Once the electricity demand has been met, the TES system can be charged with additional thermal solar energy. Then, the TES device discharges and supplies power to the steam generator to increase the amount of superheated steam generated during the peak periods to compensate the increased demand for the load. Accordingly, TES can reduce the time and rate mismatch between supply and demand and consequently, the dispatchability and marketability of CSP plants has been improved, enabling them to produce electricity on demand independently on solar power collection [6].

With regard to TES tank systems, a single tank TES has a series of advantages including that less land occupation and it can reduce costs by 30%, compared to the two-tank TES system that has been applied or projected in different CSP plants, which carries high capital costs due to tank construction materials [7,8]. The one-tank system requires only one storage tank, and part of high-cost molten-salt can be replaced by the addition of low-cost solid filler materials packed in the tank (packed-bed). As a result, the one-tank system provides more cost-effective options with potential cost-savings.

* Corresponding author. Tel.: +86(10)61773923; Fax: +86(10)61773877
E-mail address: duxz@ncepu.edu.cn (X. Du).

https://doi.org/10.1016/j.ijheatmasstransfer.2020.120677
0017-9310/

Nomenclature

a_s	interfacial area density, 1/m
C_f	inertial coefficient
C_p	specific heat at constant pressure, kJ/kg.K
D_p	particle size diameter, m
h	interstitial heat transfer coefficient, W/m^2.K
h_i	convective heat transfer coefficient, W/m^2.K
K	permeability of porous media, m^2
k	thermal conductivity, W/m.K
L	length of the tank, m
Pr	Prandtl number
Q	volume flow rate, m^3/h
Re_d	Reynolds number
R	inner radius of the tank, m
r	radial direction
t	time, s
T	temperature, K
u_{in}	inlet velocity, m/s
x	location along the tank axis, m

Greek symbols

ε	porosity of packed-bed region
Γ	effective thermal conductivity, W/m.K
ρ	density, kg/m^3
μ	viscosity, kg/m.s
δ	thickness, mm
δth	thermocline thickness, m

Subscripts

amb	ambient
c	charging
d	discharging
f	fluid or liquid
in	inlet
l	liquid molten-salt
low	lower limit
out	outlet
s	solid filler materials
st	stainless steel

Many experimental and numerical investigations focus on the thermal performance of packed-bed thermal energy storage systems. The performance of the thermal energy storage device is performed by Angelini et al. [9] through two-dimensional finite element heat transfer modeling. The results indicated that the vessel shape factor has a great influence on the thermocline thickness and collecting thermal efficiency. Nallusamy et al. [10] discovered that the hybrid thermal storage system accomplished better performance in comparison to a conventional sensible thermal energy storage device through executing experimental measurements on a storage unit incorporated with fixed and variable heating sources.

Two distinct, transient, two-dimensional models [11,12] were developed to study the discharge performance of a molten-salt packed-bed thermal energy storage system. The influences of the thermocline thickness as well as the influences of the solid particles-properties have been discussed. Yin conducted experimental and numerical investigations on thermocline characteristics of a molten-salt packed-bed tank filled with two different filler materials, namely zirconium ball and silicon carbide [13,14]. He concluded that a higher thermocline thickness was achieved by a hybrid storage device.

The operating temperature range is the most prevalent parameter in the assessment of discharge efficiency [15]. Brush et al. [16] experimentally investigated the effects of cut-off dimensionless temperature criteria on the system utilization rate through the cyclic operation of the packed-bed thermal storage system. Also, Zhao et al. [17] found that the partial charging cycles lead to further thermocline development and a strong impact on the thermal energy storage capacity in the subsequently full charging cycles. Cascetta et al. [18] carried out a comparison between experimental and numerical results of solid packed-bed under cyclic operation. It is found that the hottest area at the end of each charging phase gradually decreased by increasing the number of cycles. The effects of increasing the cut-off temperature of charging and discharging on the thermal behavior of multi-layer storage units have been investigated [19]. The maximum permissible level of the charging cut-off temperature is always associated with the size of the packed-bed. Yang and Garimella [20] concluded that Reynolds number, filler diameter, and length ratio significantly affect the cycle efficiency by performing a numerical study of the cyclic behavior of molten-salt tank, which is integrated into CSP plants. Meng et al. [21] investigated the cyclic thermal performance of a traditional single-layer and a novel multi-layer packed-bed molten-salt thermocline tank. The optimized multi-layered system shows a significant improvement in the useful energy and a small decrease in thermal efficiency in the discharging process compared to the single-layer quartzite rock system.

Some numerical studies also focused on the performance of the thermocline tank by adopting the phase change material (PCM) as part of the storage media. For low-temperature applications, the evolution of thermal stratification, as well as feasibility analysis of single charge/discharge performance of a water thermocline tank packed with paraffin wax capsules, were carried out experimentally by He et al.[22,23]. The performance of a water tank using paraffin wax is not as effective as the water tank alone, but when operating at lower flow rates the merits of a paraffin wax packed bed are evident. The cyclic operation performance of the water storage tank with PCM packed bed is strongly dependent on the completeness of charging/discharging [24]. Wu et al. [25] found that an increase in the discharge flow rate of HTF leads to a reduction in the time required for complete solidification, resulting in an increase in heat released rate when studied the discharging performance of a TES system filled with PCM spherical capsules. Du et al. [26]carried out an experimental study on the PCM-water thermocline tank under simultaneous operation. He concluded that the flow rate ratio is a good performance parameter to predict the discharging performance.

For high-temperature applications, Nithyanandam et al. [27] provided an optimum design of a latent thermal energy storage tank which uses a molten-salt as a phase change material. The enthalpy-porosity technique is utilized to simulate the solidification and melting process of PCM inside spherical capsules with different modes of operation. The unsteady characteristics of a multi-layer high-temperature packed-bed energy storage system filled with the PCM capsules are numerically investigated by Elfeky el al.[28]. PCMs layers arranged in the thermocline tank according to melting temperatures starts from high, medium, and low. It is found that, during the charging process, multi-layers PCMs melts much earlier than the single-layer system. The overall efficiency of the multi-layer packed-bed system is better than that of a single layer at the same operating conditions.

From the literature review, it can be concluded that the major efforts have been made to address the following aspects to enhance the thermal performance of a packed-bed thermocline tank [28-32], including that of the thermal performance investigation of thermocline tank using different HTFs, the operational strategies of the tank and the optimization of filler materials. However, only a few studies focus on improving the thermal performance of a packed-bed thermocline tank by controlling the evolution of thermocline as well as feasibility analysis of the thermocline tank.

Table 1
Simulation parameters of the numerical model.

Variables	Value
R	450 mm
δ_1	6 mm
δ_2	30 mm
L	1100 mm
T_{amb}	20 °C
h_i	7.8156 W/(m^2.K)
Dp	10 mm

The objective of this work is to study the dynamic thermal characteristics of a single-layered packed-bed thermocline tank by testing various solid filler materials based on the local non-equilibrium thermal theory. A detailed numerical model is developed to simulate the charging and discharging processes. The influences of the inlet flow rate and the diameter of the spherical particles on the thermocline thickness and the discharging performance of various molten-salt packed-bed energy storage systems are firstly analyzed, followed by quantitative details on the percentage increase in thermocline thickness by comparing the various single packed-bed systems with a pure molten-salt tank.

2. Numerical modeling of the molten-salt packed-bed TES system

2.1. System modeling

The current study deals with a sensible thermal energy storage packed-bed system which is applicable for high-temperature CSP plants. The storage unit is filled with stationary solid particles of solid filler arranged randomly inside the tank with a molten-salt. Two outlets are equipped with the tank for ensuring the fluid flow of molten-salt to or from the tank. The possible use of low-cost solid filler as a storage medium results in reducing the amount of molten-salt used as well as the thermal energy storage capacity increases.

As shown in Fig. 1(a), in a thermocline tank, the hot and cold fluids are stored in a single tank, during the charging process, the hot fluid enters from the top and heats the low-cost filler and leaves the bottom. While the cold fluid is entering the tank from the lower end and absorbs heat from the filler and exits from the top directly to the steam generator during the discharge process [27]. The thermocline tank used in the present study is a vertical cylindrical stainless-steel tank of 0.9 m inner diameter and 1.1 m height manufactured of a stainless steel sheet of 0.006 m in thickness [24]. The tank is equipped with spiral nozzles (distributors) to better ensure uniform distribution of molten-salt flow in the packed-bed.

Based on the above system described, a physical model is established as illustrated in Fig. 1(b), in which R is the radius of the tank, δ_1 is the thickness of the stainless steel tank, δ_2 is the thickness of the insulation layer. Considering its symmetry, only half of the packed-bed tank is taken as the numerical model. The main parameters of the numerical model are listed in Table 1.

2.2. Mathematical model

The thermal energy storage modeling of a packed-bed system can be divided into two different theories [33]. The first theory is based on thermal equilibrium, of which the solid and liquid phases are treated as a homogeneous system and yielding to a single-phase model. The second theory is based on a local non-equilibrium thermal model, in which the packed-bed modeling is represented by the two-phase model. Two coupled energy equations are solved to describe the heat transfer analysis, one for heat transfer fluid (HTF), while the second for solid materials. In this study, the local non-equilibrium thermal model is employed.

The following assumptions are employed in the present modeling [11],

(1) The fluid flow of molten-salt is considered laminar and incompressible.
(2) The top and the bottom surfaces of the thermocline tank are considered being adiabatic.
(3) The fluid flow and heat transfer along the axis are considered to be axisymmetric, so the governing transport equations inside the tank become two-dimensional.
(4) There are no distributors in the computational domain and uniform flow is imposed at the inlet and outlet.
(5) The conical bottom of the tank is not included in the computational domain, so the finalized shape of the domain under study is the cylindrical part only of 1.1 m length.
(6) The properties of solid fillers remain constant.
(7) Filler materials are spherical capsules treated as a continuous, homogenous, and isotropic porous medium, and the heat conduction between filler particles is neglected due to high inter contact resistance.
(8) Radiation heat transfer between the fluid and solid, and between particles in the bed is neglected.

With the above assumptions, the Navier-Stokes equations with the two-energy equations are employed to describe the fluid flow and heat transfer characteristics corresponding to the computational domain illustrated in Fig. 1(b).

- Continuity equation

$$\frac{\partial(\varepsilon\rho_l)}{\partial t} + \nabla\cdot\left[\rho_l\vec{u}\right] = 0 \tag{1}$$

where ρ_l is the molten-salt density and $\vec{u}$ is the superficial velocity vector.

- Momentum equation

$$\frac{\partial\left(\rho_l\vec{u}\right)}{\partial(\varepsilon t)} + \frac{\nabla\cdot\left[\rho_l\vec{u}\,\vec{u}\right]}{\varepsilon^2} = \nabla\cdot\left(\mu\nabla\vec{u}\right) - \nabla P + \rho_l\vec{g} - \left(\frac{C_F\rho}{\sqrt{K}}|\vec{u}|\right)\vec{u} \tag{2}$$

where C_F is the inertial loss coefficient, and K is the porous medium interstitial permeability and these parameters can be calculated from the following relations as reported in [34].

$$C_F = \frac{3(1-\varepsilon)}{D_p\varepsilon^3} \tag{3}$$

$$K = \frac{D_p^2\varepsilon^3}{150(1-\varepsilon)^2} \tag{4}$$

where ε is the porosity of the packed-bed zone, and D_p is the spherical particle diameter.

- Energy balance equation for the molten-salt

$$\frac{\partial\left(\varepsilon\rho_l C_{p,l}T_l\right)}{\partial t} + \nabla\cdot\left[\rho_l C_{p,l}\vec{u}\,T_l\right] = \nabla\cdot\left(\Gamma_{l,eff}\nabla T_l\right) + a_s\,h(T_s - T_l) \tag{5}$$

where T_s and T_l represent the temperatures of solid particle size and the molten-salt respectively, $\Gamma_{l,eff}$is the effective thermal conductivity of the molten-salt, $C_{p,l}$ is the specific heat capacity of the molten-salt.

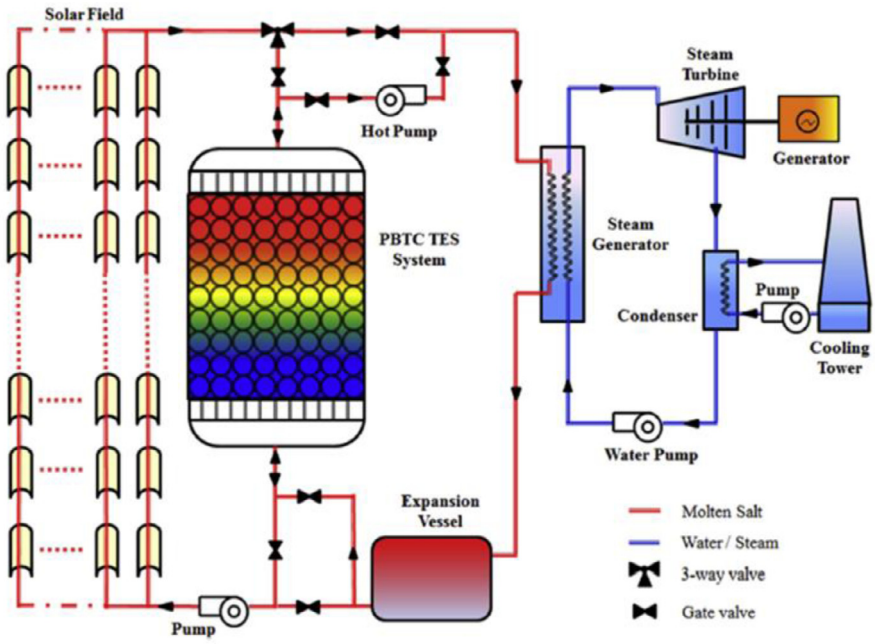

(a) Molten-salt packed-bed thermocline storage tank integrating with CSP plant [15].

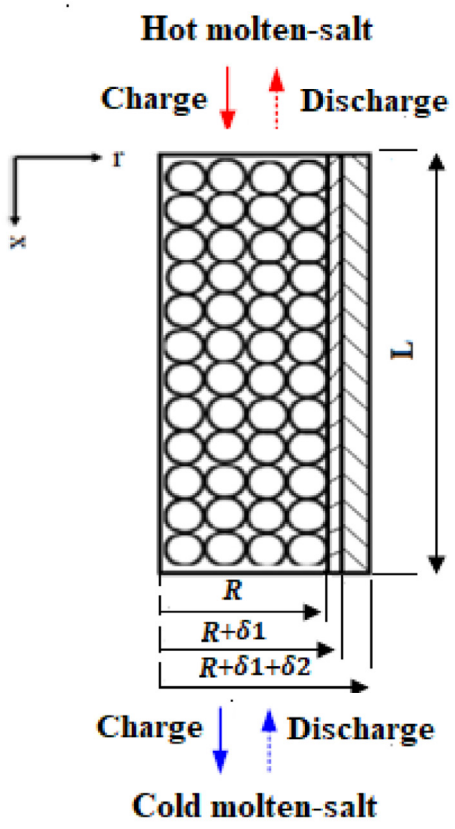

(b) Numerical model.

Fig. 1. Physical model. (a) Molten-salt packed-bed thermocline storage tank integrating with CSP plant [15]. (b) Numerical model.

- Energy balance equation for the solid filler

$$\frac{\partial((1-\varepsilon)\rho_s C_{p,s} T_s)}{\partial t} = \nabla \cdot \left(\Gamma_{s,eff} \nabla T_s\right) - a_s\, h(T_s - T_l) \tag{6}$$

where ρ_s and $C_{p,s}$ are the density and specific heat capacity of the solid filler particles, $\Gamma_{s,eff}$ is the solid thermal conductivity.

The above energy balance equations are coupled by the interstitial heat transfer coefficient h between the heat transfer fluid and interfacial area density a_s. The heat transfer coefficient h is a function of Reynolds number and Prandtl number and it determines from the following correlation reported in [35].

$$h = k_l\left[2 + 1.1\mathrm{Re}_d^{0.6}\mathrm{P_r}^{1}/3\right] \tag{7}$$

where Re_d is the Reynolds number based on the effective filler diameter D_p, and interfacial area density a_s which calculated from the following relation [15]:

$$a_s = \frac{6(1-\varepsilon)}{\mathrm{D_p}} \tag{8}$$

- The energy equation for the outer thermal insulation layer and steel tank wall thickness

$$\frac{\partial\left(\rho_i C_{p,i} T_i\right)\mathrm{i}}{\partial t} = \nabla \cdot (\Gamma_i \nabla T_i) \tag{9}$$

where i means the tank steel wall and insulation layer. The heat is transferred by conduction through the insulation layer and steel wall thickness.

- The boundary conditions

For the charging process at the inlet:

This boundary represents the inlet of hot molten-salt at which both the inlet velocity and temperature specified to be inlet conditions,

$$\begin{aligned} &x = 0,\ 0 \le r \le R \\ &u|_{+} = u_{in},\ T_f\big|_{+} = T_{in,f},\ \partial T_s/\partial x|_{+} = 0 \end{aligned} \tag{10}$$

For the charging process at the outlet:

This boundary represents the outlet of cold molten-salt with the following conditions,

$$\begin{aligned} &x = L,\ 0 \le r \le R \\ &\partial u/\partial x|_{-} = 0,\ \partial T_f/\partial x\big|_{-} = 0,\ \partial T_s/\partial x|_{-} = 0 \end{aligned} \tag{11}$$

For the discharging process,

$$\begin{aligned} &x = 0,\ 0 \le r \le R, \\ &\partial u/\partial x|_{+} = 0 = 0,\ \partial T_f/\partial x\big|_{+} = 0,\ \partial T_s/\partial x|_{+} = 0 \end{aligned} \tag{12}$$

and,

$$\begin{aligned} &x = L,\ 0 \le r \le R, \\ &u|_{-} = -u_{in},\ T_f\big|_{-} = T_{in,f},\ \partial T_s/\partial x|_{-} = 0 \end{aligned} \tag{13}$$

When $0 \le x \le L$, $r = 0$:

This boundary represents the symmetry axis of the cylindrical tank, at which symmetrical boundary conditions are employed to the fluid and solid filler temperatures and u-velocity of fluid, while the v-velocity of fluid is set to be zero:

$$\partial u/\partial r|_{+} = 0,\ v|_{+} = 0,\ \partial T_f/\partial r|_{+} = 0,\ \partial T_S/\partial r|_{+} = 0 \tag{14}$$

When $0 \le x \le L$, $r = R + \delta_{1+}\ \delta_2$:

This boundary represents the outer surface of the storage tank exposed to the ambient conditions. Forced convection heat transfer from the surface to the ambient air and the following boundary condition is as follow;

$$-k\frac{\partial T}{\partial r}\bigg|_{-} = h_i(T - T_{amb}) \tag{15}$$

where the convective heat transfer coefficient calculated from a correlation over a flat plate surface was reported in [11], by setting the ambient air velocity of 5m/s.

When x=0 or x=L, $R \le r \le R + \delta_{1+}\ \delta_2$:

These boundaries represent the cross-sections of the tank wall and outer insulation layer adjacency to the fluid outlet and inlet at which adiabatic conditions are assumed:

$$\partial T_{\delta 1}/\partial x = \partial T_{st}/\partial x = 0 \tag{16}$$

2.3. Material properties of solid packed-bed TES

With respect to the molten-salt, it is consists of a mixture of 60 wt% $NaNO_3$ and 40 wt% KNO_3 and the thermo-physical properties characterized by the following equations where T in °C [36].

$$\rho_l = 2090 - 0.636 \times T \tag{17}$$

$$C_{p,l} = 1473 + 1.72 \times T \tag{18}$$

$$k_l = 0.443 + 1.9 \times 10^{-4} T \tag{19}$$

$$\mu_l = \left[22.714 - 0.12 \times T + 2.281 \times 10^{-4} T^2 - 1.474 \times 10^{-7} \times T^3\right] \times 10^{-3} \tag{20}$$

Three important filler materials are selected as the packed solid thermal energy storage medium. Among them, the sintered slag pebbles have the following characteristics where T in °C according to H2020 RESLAG project described in [37],

$$C_{p,s} = 827.69 + 0.3339T \tag{21}$$

$$k_s = 1.6792 - 5.3237 \times 10^{-4} T \tag{22}$$

The density of slag pebbles does not depend on the temperature compared to other properties and it has a fixed value of 2850 kg/m^3.

The European steel industry generated about 21.4 million tons of slag in 2012 resulting from steel-making. About 24% is not being reused, representing a severe environmental problem in Europe, but also a huge amount of available material for potential recycling. RESLAG will face this environmental problem by providing 4 eco innovative industrial alternative applications to valorize the steel slag that is currently not being recycled. Among alternatives, the possible use of slag pebbles as a storage medium in thermal energy storage system integrated in CSP plants. Slag pebbles can withstand up to 1100 °C before melting, but considering the steel construction material of the storage tank and the operating temperatures of molten-salt used in this study, we are limiting this application to 500 °C.

The physical properties of the other solid fillers are scheduled in Table 2. The packed-bed porosity considered in the whole study is about of 0.379, referring to a similar consideration as Refs. [11,12].

2.4. Numerical simulation and model validation

The finite volume method is used to numerically solving the governing equations using Ansys FLUENT 19.1 solver by compiling a comprehensive UDF code for a solid-packed bed in the porous zone. The pressure-velocity coupling field is solved by the SIMPLE algorithm. The momentum equation and two energy equations are both discretized by the second-order upwind scheme. The convergence criteria of the continuity equation, momentum equation, and energy equations are 10^{-3}, 10^{-3}, and 10^{-9}, respectively.

Table 2
Physical properties of various solid fillers.

Material	Density (kg/m^3)	Specific heat capacity (J/kg.K)	Thermal conductivity(W/m.K)
Quartzite rock	2500	830	5.69
Alumina ceramics	3750	780	30

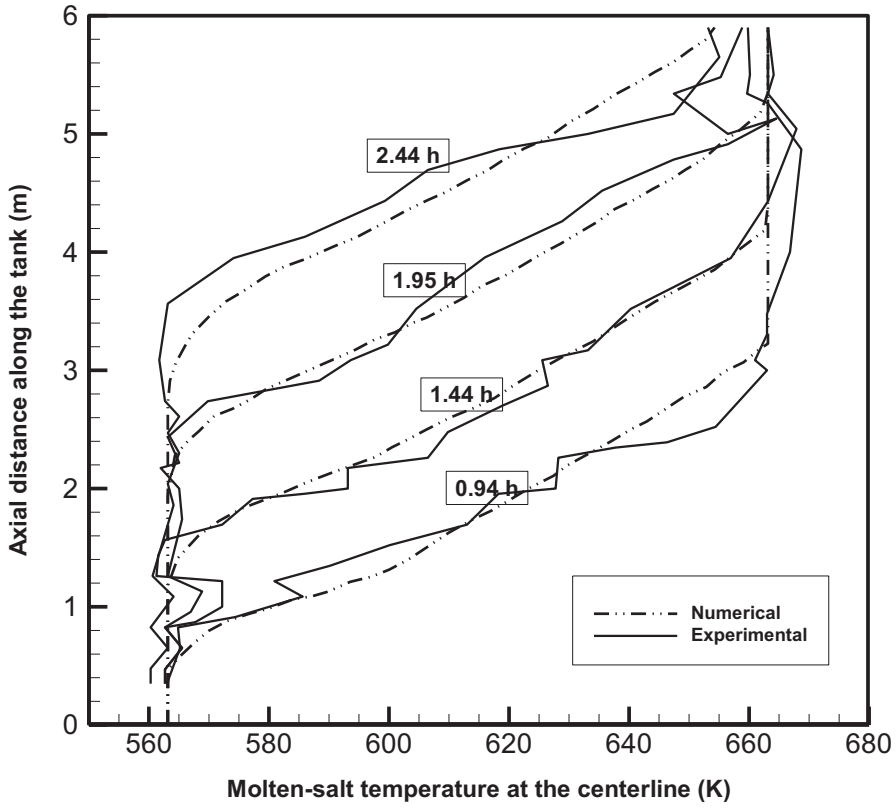

Fig. 2. Comparison of simulation and experimental results of Q_d=10.652 m^3/h, T_c=663.15 K, T_d=563.15 K during the discharging process.

To guarantee that the results obtained from the numerical model are independent on the grid size, three uniform grids with various grid sizes (number of cells) of 495000 (fine), 220200 (medium), and 123750 (coarse) are used in this study, by maintaining the time step length constant at 1s and the max iterations of 20 for each time step. The results indicate that there is no significant difference in the temperature values for all cases that ensure the solution of the present model is not mesh dependent. So, the medium grid size is used in this study each cell size of (1.5 × 1.5) mm^2 for further simulations due to its computational effective economic.

The validation of the present model is performed based on the experimental data reported by Pacheco et al. [8]. The numerical results are compared with the experimental results that were carried out at the same operating conditions of Q_d= 10.562 m^3/h, T_c =663.15 K, T_d=563.15 K, and porosity of 0.22 during the discharging process.

Fig. 2 illustrates the experimental and numerical variations in the axial temperature profiles of molten-salt at the centerline of the storage tank. It is observed that the simulation results seem to be in a reasonable agreement with the experiments with slight deviations of the experimental curves at the inlet and outlet, this may be due to the uncertainties in the measurement process and the possible existence of a vortex which is formed by flowing molten-salt through a storage unit.

3. Results with analysis

The dynamic thermal characteristics of the thermal energy storage system are the key factors to determine the power generation and efficiency of the CSP plants. This section addresses the influences of the inlet flow rate and the diameter of the spherical particles on the thermocline thickness, as well as the discharging performance of different materials properties. In addition, the analysis includes comparisons between the various packed-bed systems and the pure molten-salt tank.

3.1. General thermal behavior with a single discharging process

Fig. 3 illustrates thermocline evolution and two-dimensional temperature contours inside the molten-salt tank for both cases with and without solid packed-bed. The temperature contours were produced during the discharging process for a temperature range of 663.15/563.15 K and Q_d=0.3 m^3/h, respectively. The packed-bed tank is filled with slag pebbles as a filler with a spherical particle size of 1 cm and a porosity of 0.379.

The thermocline thickness, δ_{th}, is an important criterion for the thermal energy storage performance in a packed-bed tank. The thermocline thickness can be calculated according to the upper and lower limits of temperature gradients according to the follow-

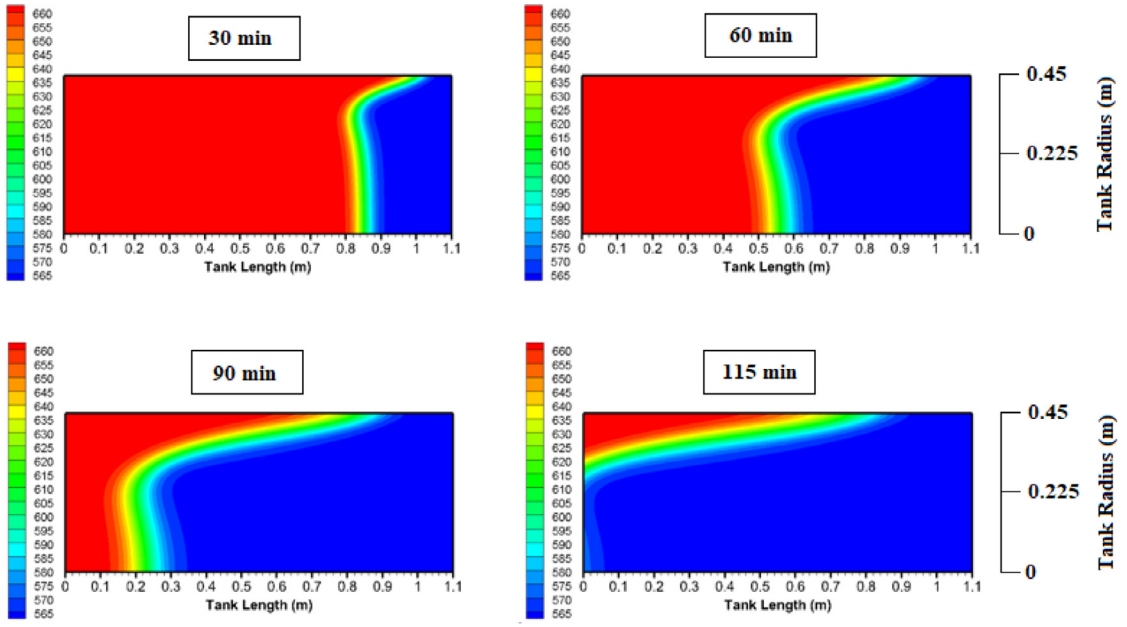

(a) Molten-salt tank.

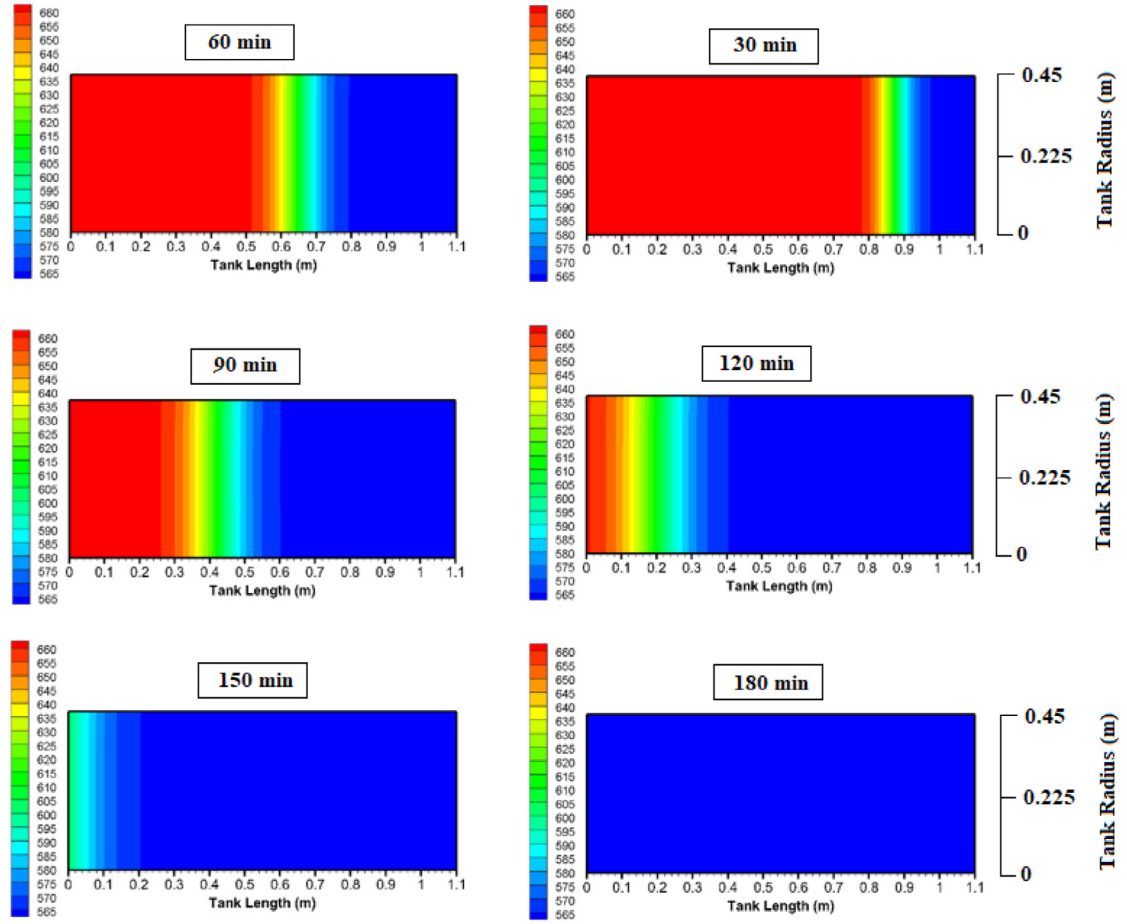

(b) Packed-bed tank.

Fig. 3. Two-dimensional temperature distribution and thermocline evolution during the discharging process for a flow rate of 0.3 m^3/h and temperature range of T_c=663.15 K, T_d=563.15 K. (a) Molten-salt tank. (b) Packed-bed tank.

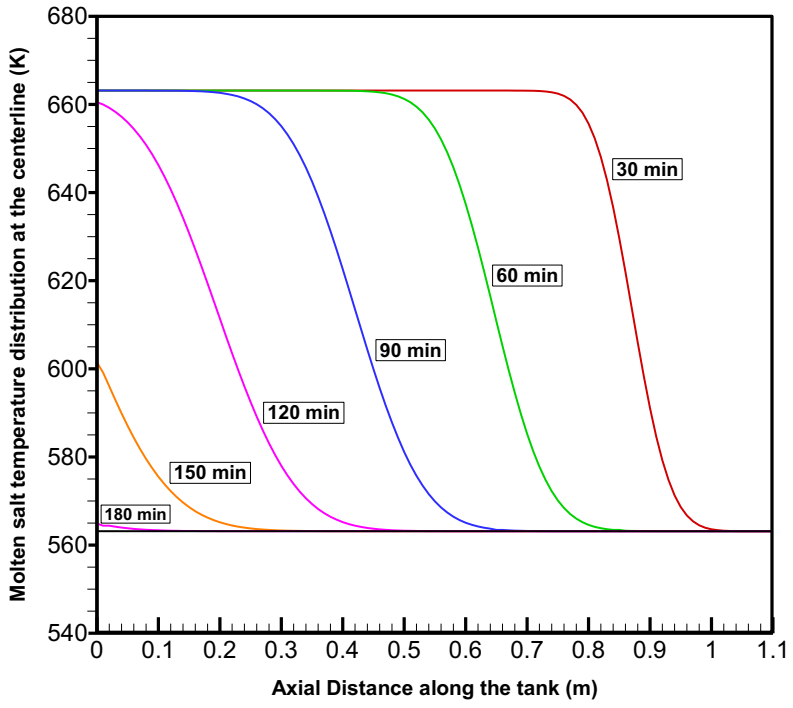

(a) Axial temperature distribution profiles at different time instants during the discharging process.

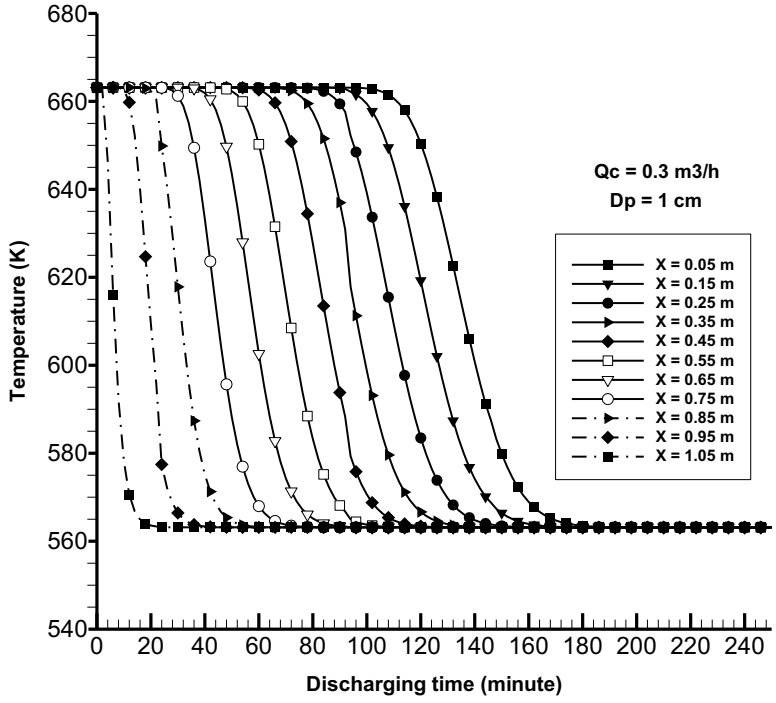

(b) Variations in packed-bed temperature field of each level with discharging time during the discharging process for a flow rate of 0.3 m^3/h and temperature range of T_c=663.15 K, T_d=563.15 K.

Fig. 4. Comprehensive temperature field of packed-bed inside the storage device. (a) Axial temperature distribution profiles at different time instants during the discharging process. (b) Variations in packed-bed temperature field of each level with discharging time during the discharging process for a flow rate of 0.3 m^3/h and temperature range of T_c=663.15 K, T_d=563.15 K.

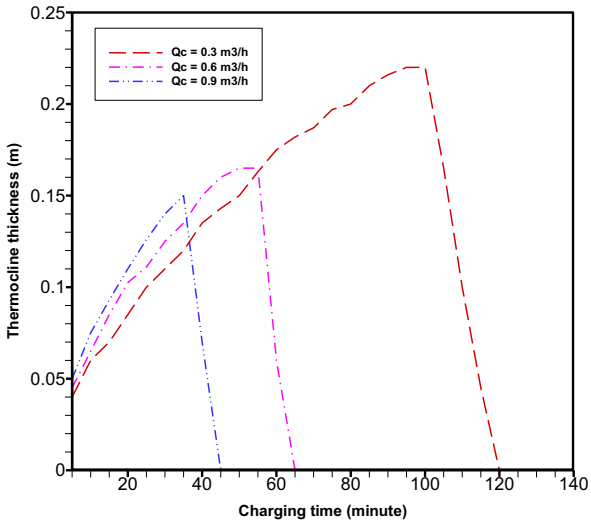

(a) Molten-salt tank.

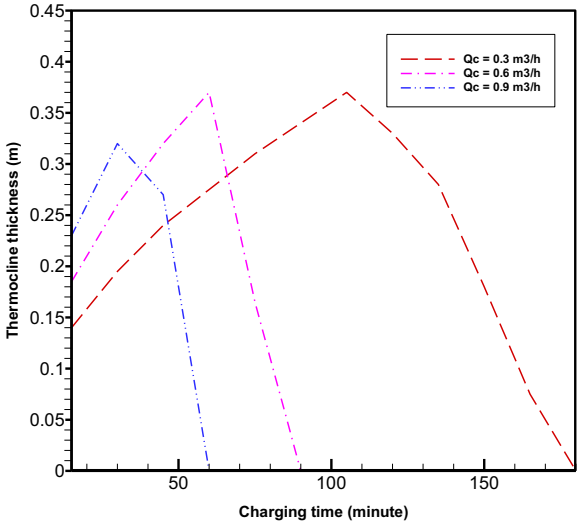

(b) Packed-bed tank, slag pebbles.

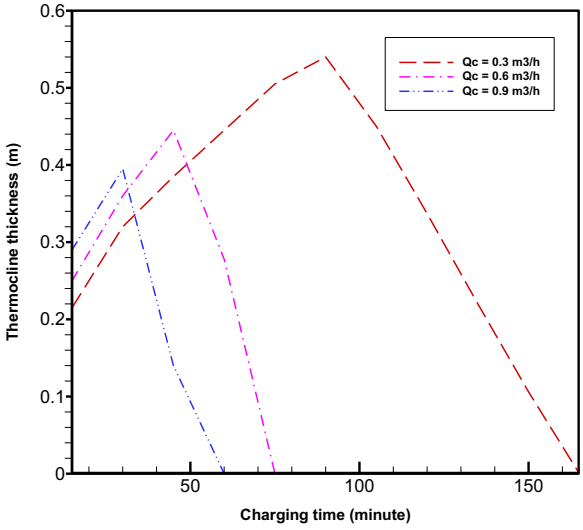

(c) Packed-bed tank, quartzite rock.

Fig. 5. Influences of HTF inlet flow rate on thermocline thickness. (c) Packed-bed tank, quartzite rock. (a) Molten-salt tank. (b) Packed-bed tank, slag pebbles

Table 3
The time required for complete charging process for various packed–bed systems.

TES system	Q_c (m^3/h)	porosity	Particle size (cm)	Time of charging (min)
Molten-salt tank	0.3	–––	–––	140
	0.6	–––	–––	70
	0.9	–––	–––	48
Slag pebble	0.3	0.379	1	250
packed-bed system	0.6	0.379	1	125
	0.9	0.379	1	85
Quartzite rock	0.3	0.379	1	240
packed-bed system	0.6	0.379	1	120
	0.9	0.379	1	80
Alumina ceramics	0.3	0.379	1	550
packed-bed system	0.6	0.379	1	275
	0.9	0.379	1	184

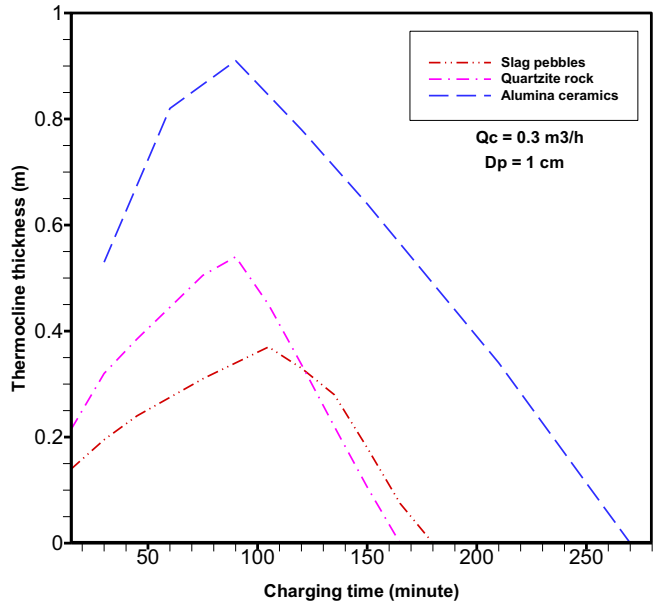

(a) Packed-bed of three various fillers.

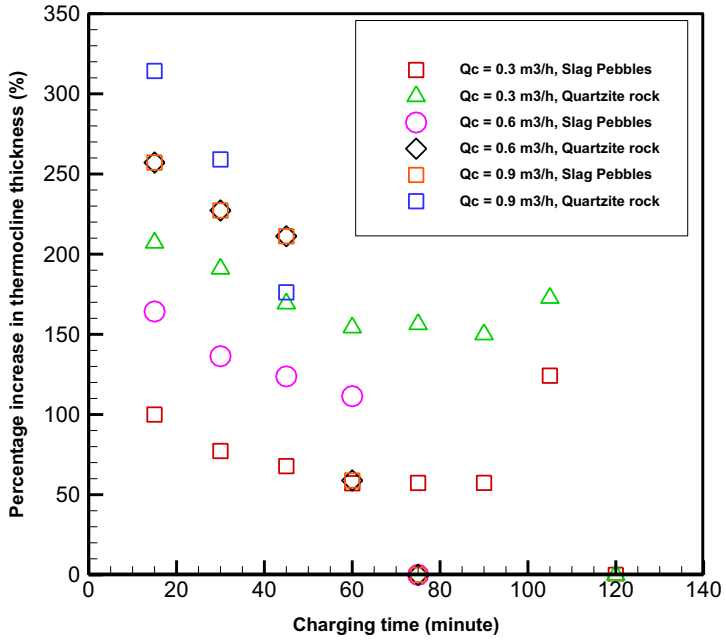

(b) Variations in percentage increase of thermocline thickness for various packed bed systems.

Fig. 6. Influences of packed-bed fillers on thermocline thickness. (a) Packed-bed of three various fillers. (b) Variations in percentage increase of thermocline thickness for various packed bed systems.

ing equation as in [14],

$$\delta_{th} = x_h - x_l = (L - u_{in}.t) - x_l \tag{23}$$

where L is the thermal energy storage zone length, u_{in} is the inlet velocity, t is the time and x_l is the axial height on the lower boundary limit.

Generally, the thermocline of the molten-salt tank is completely different from the packed-bed in terms of pattern, evolution trend, thickness, and time required for complete discharging. It can be observed that the evolution of a thin thermocline layer close to the tank wall in the case of molten-salt tank forms once discharging starts. Both the length and thickness of this layer expand with time which resulted in a little amount of cold-molten salt adjacent to the wall that did not reach the high-temperature level compared to centerline temperature. The phenomena can result from three causes. The first one due to the formation of the velocity bound-

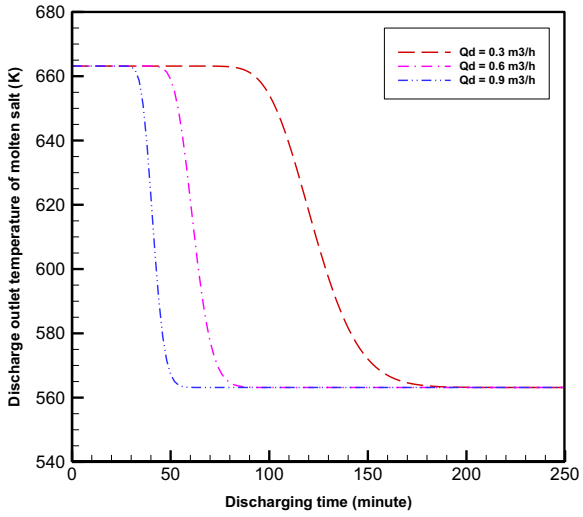

(a) Discharge outlet temperature, quartzite rock

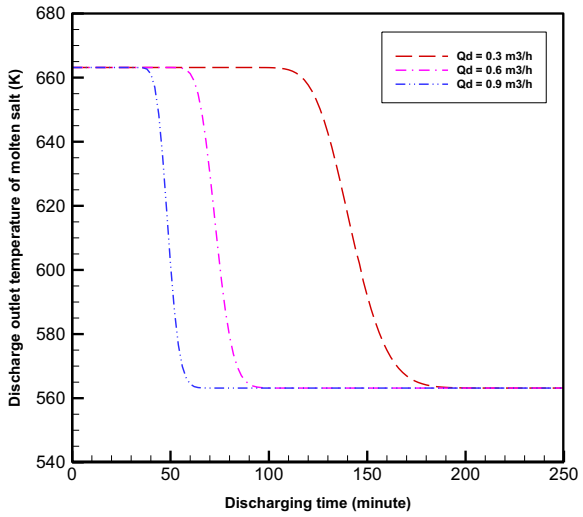

(b) Discharge outlet temperature, slag pebbles

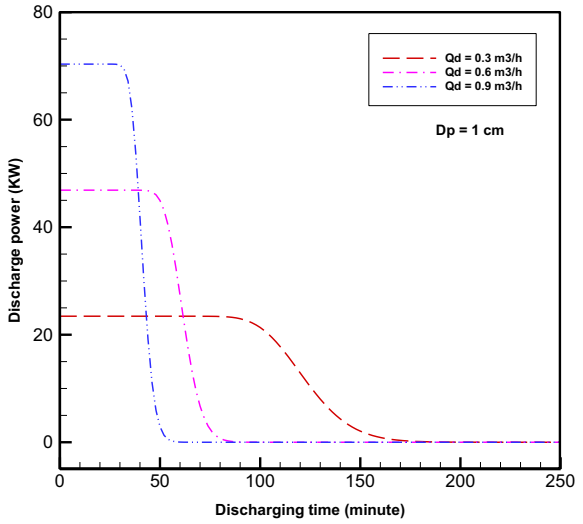

(c) Discharge power, quartzite rock

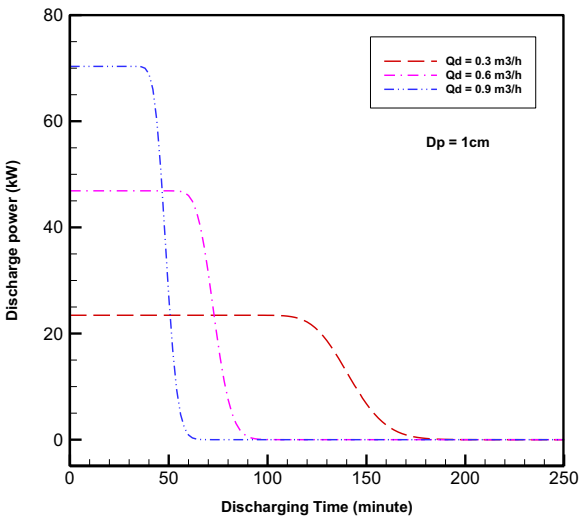

(d) Discharge power, slag pebbles

Fig. 7. Variations in (a) Discharge outlet temperature of quartzite rock. (b) The discharge outlet temperature of slag pebbles. (c) Discharge power of quartzite rock. (d) Discharge power of slag pebbles. (a) Discharge outlet temperature, quartzite rock (b) Discharge outlet temperature, slag pebbles (c) Discharge power, quartzite rock (d) Discharge power, slag pebbles.

Table 4
Complete discharging time for different particle diameters.

Material type	Particle size (cm)	Time of complete discharging (min)
Slag Pebbles	1	114
	2	136
	3	158
	4	180
Quartzite rock	1	112
	2	126
	3	142
	4	158

ary layer existence near the wall, which caused by hot molten-salt entering the storage tank from the top. The second reason, owing to the cold fluid stagnation near the tank wall results in a larger temperature gradient. Besides, employing heat dissipation boundary conditions at the outer wall leads to a faster temperature drop of HTF near the tank wall, so this factor also can contribute to forming a temperature gradient. On the contrary, a thermocline thickness layer along the tank radius maintains the same in the case of the packed-bed tank, which means the charge outlet temperature remains constant at different radial positions by the end of the discharging process.

It is clear from the contour map that, a packed-bed tank achieves a thicker thermocline layer than that of the molten-salt tank. So, the latter shows better thermal stratification performance than the packed-bed tank. This is maybe due to the expansion of the thermal gradient zone inside the tank as a result of the axial heat conduction between the slag pebbles and molten-salt through the packed-bed. Additionally, the increased thermal resistance be-

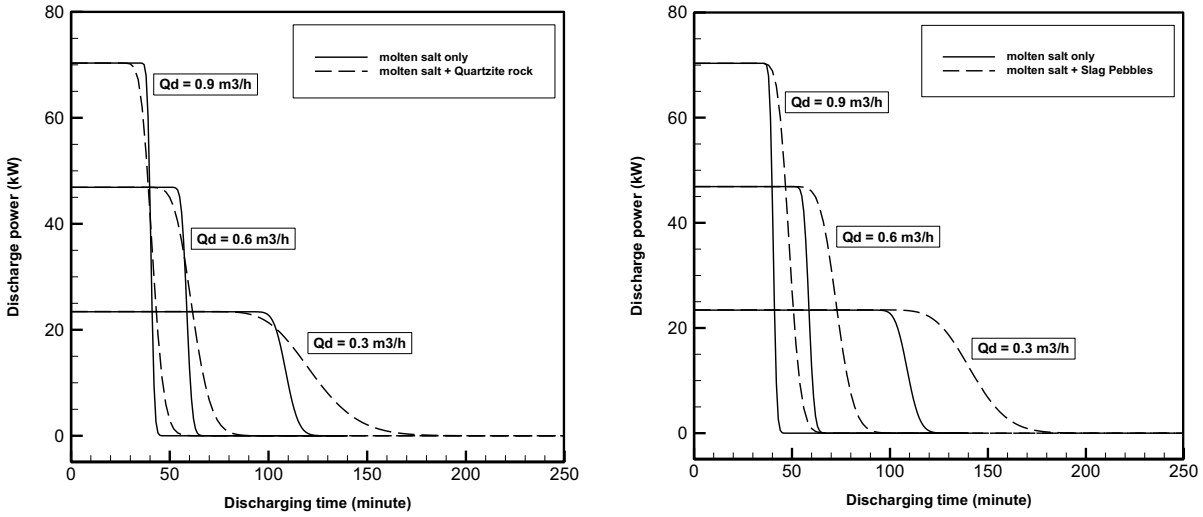

(a) Discharge power comparison of quartzite rock packed-bed and pure molten-salt system.

(b) Discharge power comparisons of slag pebbles packed-bed and pure molten-salt system.

Fig. 8. Variations in discharge power comparisons for various storage packed-bed systems compared to pure molten-salt. (a) Discharge power comparison of quartzite rock packed-bed and pure molten-salt system. (b) Discharge power comparisons of slag pebbles packed-bed and pure molten-salt system.

tween salt and filler material results in a decreasing heat exchange rate, and consequently, the thermal gradients increases.

All these reasons give a significant indication of poorer stratification behavior for the packed-bed tank. It also can be acquired by comparing Fig. 3(a) and (b) that the use of slag pebbles with molten-salt leads to an increase in the thermal energy storage capacity, which takes almost one and a half of the time required for complete discharging compared to the pure molten-salt tank.

A comprehensive temperature field of the packed-bed tank has been plotted against both axial positions and time of discharging as shown in Fig. 4 (a) and (b), respectively. In Fig. 4(a), one can observe that the molten-salt temperature profile at the centerline gradually declines with time from the high-temperature value of 663.15 K until reaches to lower one of 563.15 K. This indicates indirectly that thermocline thickness increases continually with time by a subsequent decrease of the hottest area inside the tank that agrees with the former discussion [14].

Fig. 4 (b) presents the axial temperature variations of molten-salt with the discharging time of each layer inside the packed-bed tank. The thermal energy storage tank is divided into 11 axial levels from top to bottom. The temperature profile of each layer in Fig. 4 (b) consists of three zones including that of (1) constant low-temperature zone, (2) constant-high temperature zone, and (3) heat exchange zone as also reported in [27]. Besides, in the case of the packed-bed tank, the temperature profiles seem to be steeper than the molten-salt tank during the heat exchange zone. This is due to the thicker thermal gradients resulted from the axial heat conduction.

3.2. The effect of inlet flow rate on the dynamic thermal characteristics

This section analyses the obtained simulation results by testing a numerical model at different volume flow rates during the charging process. Three quantities of inlet flow rates of 0.3, 0.6, and 0.9 m^3/h are introduced. All the simulation runs are carried out at the same operating temperature conditions of 663.15/563.15 *K*, porosity of 0.379, and a particle size of 1 cm.

3.2.1. Thermocline thickness during the charging process

As illustrated in Fig. 5, the expansion of thermocline thickness increases as the inlet flow rate increases for various storage systems. So, the cold molten-salt needs to travel long distance inside the tank to absorb stored heat due to the presence of a higher temperature gradient which resulted in shrinking the hottest region within the tank. Besides, for all inlet flow rates, the thermocline evolution increases with time during the charging process even till it reaches the highest value. Beyond this period it begins to decline gradually until it reaches zero and the storage tank is completely charged with higher temperature.

The progressive increase in the thermocline thickness of the packed-bed tank may be due to the disturbances occurs inside the tank with increasing the flow rate, which in turn forms a thicker thermal gradient. It is noticed that the packed-bed systems achieve higher values of thermocline thickness compared to the molten-salt tank due to the axial heat conduction of various fillers. For instance, slag pebbles and quartzite rock packed-bed systems achieve a percentage increase in thermocline thickness of approximately 228% and 315%, respectively, compared to a pure molten-salt tank at a higher flow rate of 0.9 m^3/h. While these percentages for both systems decreased to 57.14% and 154.28% respectively when operating at a flow rate of 0.3 m^3/h as illustrates in Fig. 5(b) and (c).

As shown in Fig. 6(a), as far as complete charging time is concerned, alumina ceramics shall take a charging period of twice the value of quartzite rock required under the same operating conditions. Also, the thermocline thickness of this material is larger than the slag pebbles and quartzite rock. The percentage increase in thermocline thickness with reference to its value of pure molten-salt is reported in Fig. 6(b). The time required for the complete charging process for various storage systems is listed in Table 3.

3.2.2. Discharging performance

The discharge outlet temperature plays a crucial role in obtaining a steady discharge process that compensates for peaking shaving periods that cause load instability. So, the discharge temperature profiles are plotted at various flow rates to indicate the temperature stability of hot molten-salt that exists from the various

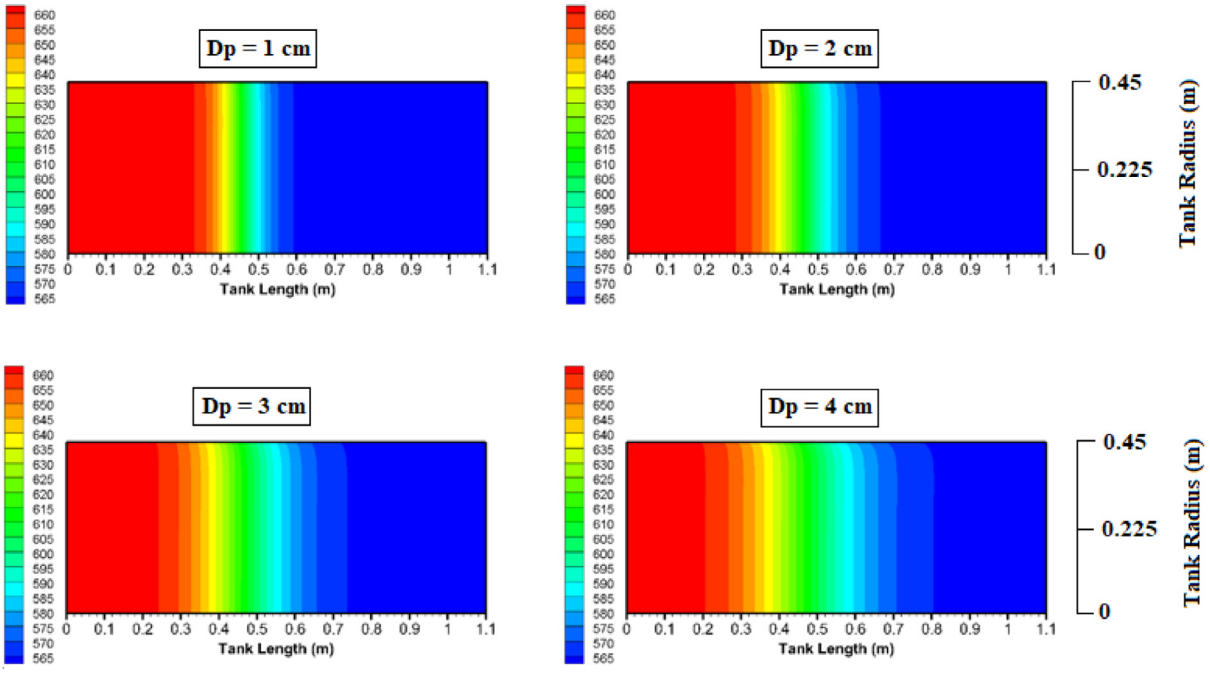

(a) For slag pebbles packed-bed, 30 min, Q_c = 0.6 m3/h.

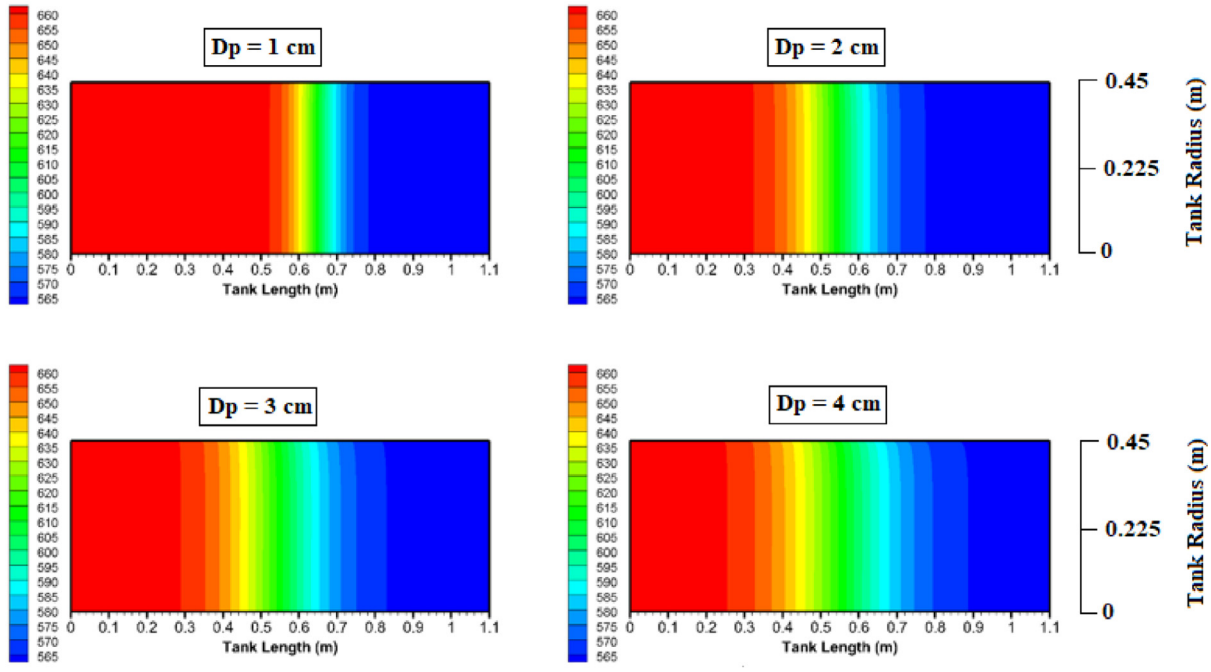

(b) For quartzite rock packed-bed, 30 min, Q_c = 0.6 m3/h.

Fig. 9. 2-D temperature distribution and thermocline evolution for two different packed-bed systems. (a) For slag pebbles packed-bed, 30 min, Q_c = 0.6 m3/h. (b) For quartzite rock packed-bed, 30 min, Q_c = 0.6 m3/h.

packed-bed systems, as shown in Fig. 7(a) and (b). It can be observed that, for both packed-bed systems, the higher the inlet flow rate, the less time the outlet temperature is to be stable for the heat-supply net. For instance, the steady-state temperature period decreases from 90 min to 30 min when the discharge flow rate increases from 0.3 m^3/h to 0.9 m^3/h, respectively, in the case of quartzite rock packed-bed. Compared to quartzite rock packed-bed, slag pebbles achieve higher discharge stability under the same operating conditions. For example, the temperature steady-state period is about 130 min while in the case of quartzite rock packed-bed is 90 min at the same operating flow rate of 0.3 m^3/h. This is due to an increase in the specific heat capacity of slag pebbles than quartzite rock and these results confirm other results reported by Cabello in [37]. The profiles of discharge power under the heat re-

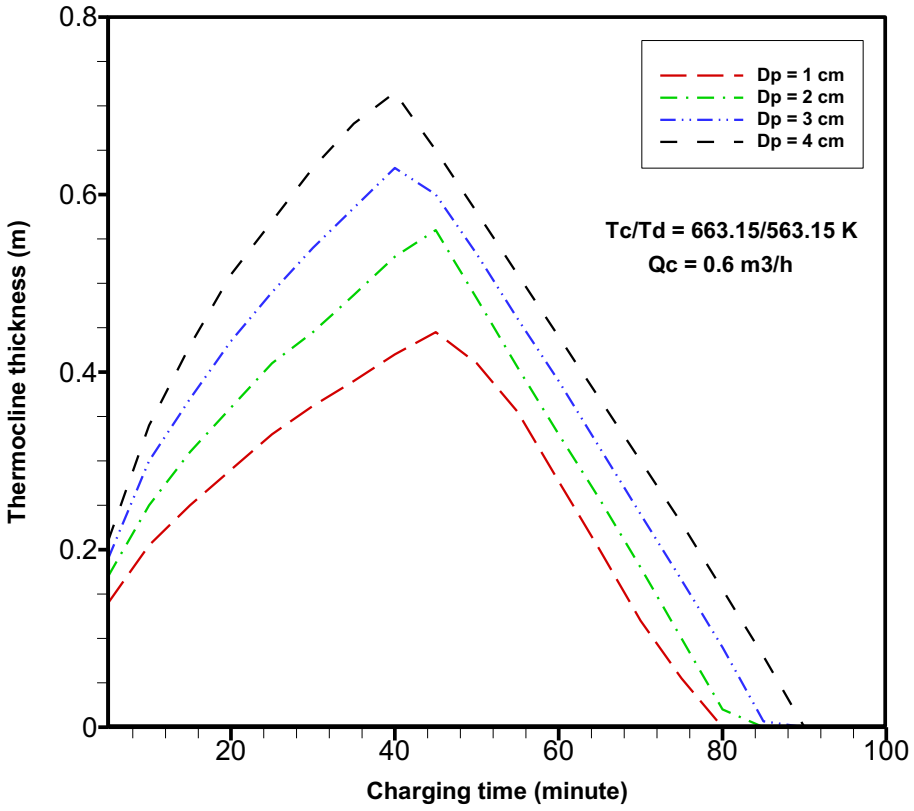

Fig. 10. Variations in thermocline thickness with charging time of a quartzite rock packed-bed for different particle diameters.

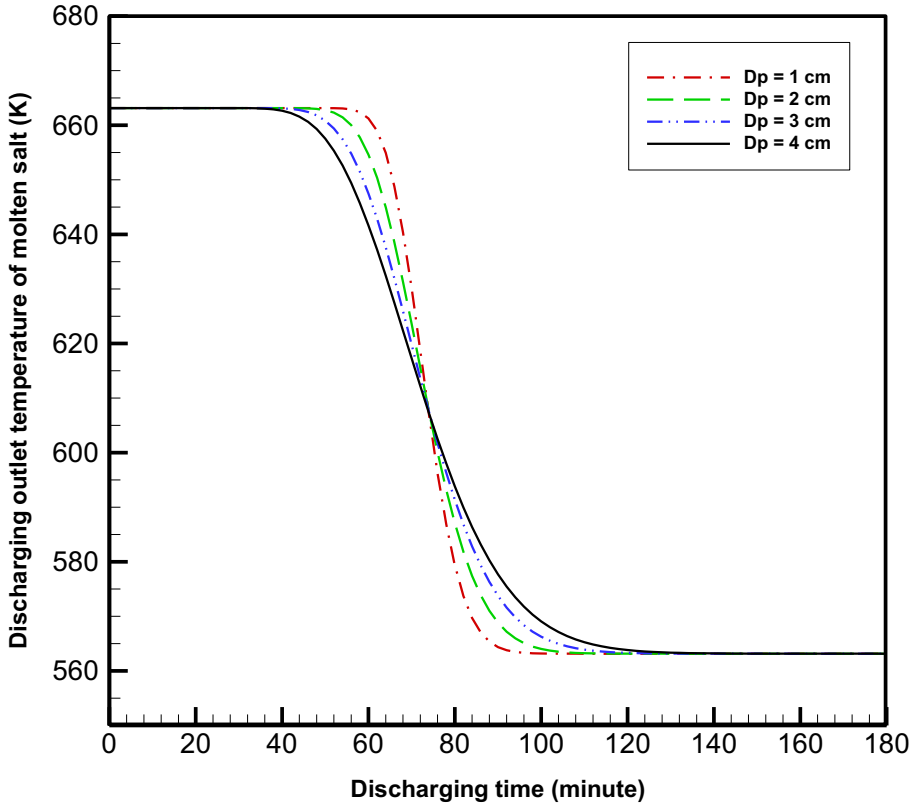

Fig. 11. Variations in discharge outlet temperature of slag pebbles packed-bed with discharging time for different particle diameters.

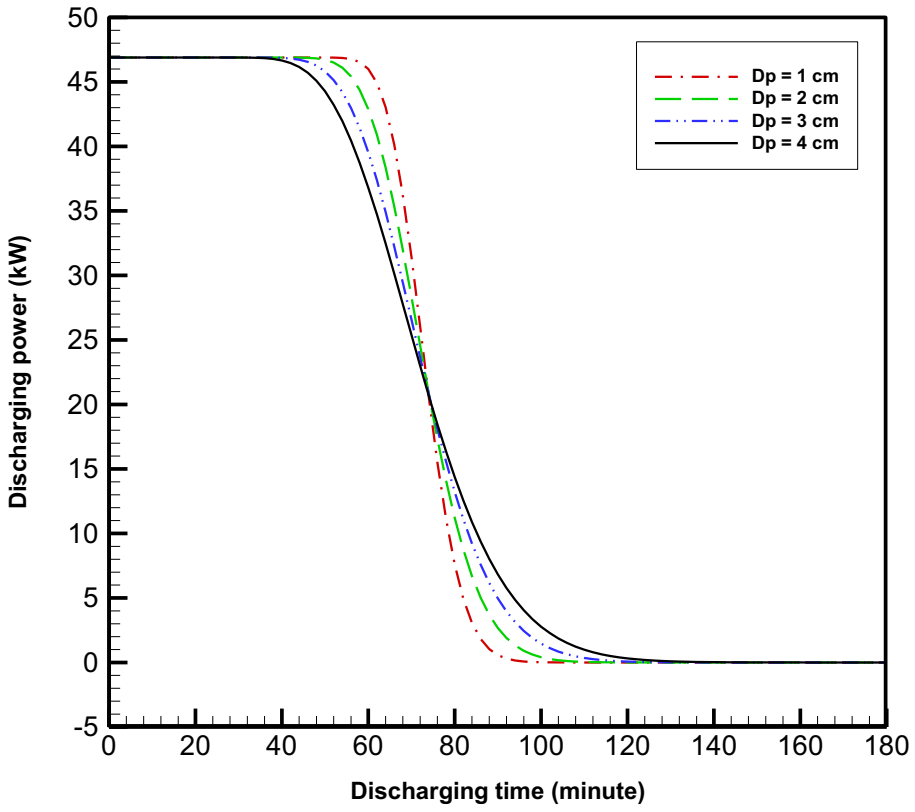

Fig. 12. Variations in discharging power of slag pebbles packed-bed with discharging time for different particle diameters.

lease process for various thermal energy storage packed-bed systems are shown in Fig. 7. (c) and (d). The discharge power is defined by the following equation:

$$P_d = \int_0^{t_d} C_{p,l} Q d \rho_l (T_{\text{out}} - T_{\text{in}}) \tag{24}$$

It depends mainly on the temperatures of the inlet and outlet, the volume flow rate, and specific heat capacity of the heat transfer fluid. As a result, the discharging power trend is similar to that of the outlet temperature. One can observe that, discharging power increases by increasing the flow rate. For instance, the discharge power increases from 23 kW to 70.3 kW as the discharge flow rate increases from 0.3 m^3/h to 0.9 m^3/h, respectively. According to a steady-state period, slag pebbles achieve a longer steady period than quartzite rock, so the discharge performance of the TES system using slag pebbles is more effective than another one used a quartzite rock.

Fig. 8 shows a comparison of the discharge power for two packed-bed systems with a pure molten-salt system. It is obvious that the discharge power increases with the increase in the flow rate. For a certain flow rate of 0.3 m^3/h, the outlet temperature of the molten-salt is stable for most of the time during the discharging process. From the perspective of the discharging power, both packed-bed tanks show better performance when the flow rate decreases to a smaller value.

3.3. The effect of spherical particle size on the dynamic thermal characteristics

The effect of the spherical particle diameter on dynamic characteristics is discussed in this section. The investigation is carried out through testing different sizes of slag pebbles and quartzite rock fillers varying from 1 to 4 cm.

3.3.1. Thermocline thickness during the charging process

Fig. 9 presents variations in the temperature distribution and thermocline evolution within the storage device along the tank axis using different particle diameters. For both packed-bed systems, with the increase in the particle diameter, the thermocline thickness increases and the effective charging time increases. With the decrease in the particle diameter from 4 to 1 cm, the system can be effectively charged for a shorter period. For instance, as the particle diameter increases from 2 cm to 4 cm, the thermocline thickness increases from 0.38 m to 0.6 m in the case of slag pebble, while its value increases from 0.45 m to 0.64 m in the case of quartzite rock. Slag pebbles packed-bed has comparatively lower thermal gradient values inside the storage unit compared to quartzite rock.

As for the thermocline thickness shown in Fig. 10, with the increase in the particle diameter from 1 to 4 cm, the thermocline expands faster, the hottest area shrinks, and the maximum thermocline thickness increases from 4.2 to 7.3 m approximately [12]. This is due to the heat transfer processes between molten salt and particle surface and within the solid particle, which is highly dependent on the particle size, which can be elaborated by referring to the trend of representative molten salt temperature distributions as illustrated in Fig. 9.

3.3.2. The effect of solid particle diameter on the discharging performance

Fig. 11 shows variations in the temperature of the molten-salt at the outlet with the discharging time using various particle diameters varying from 1 to 4 cm. As the particle size increases, the outlet temperature of the molten-salt starts to fall earlier and the effective discharging time is shortened. In addition, the time required to decrease the outlet temperature from 663.15 to 563.15 K is significantly extended. With the decrease in the particle diameter from 4 to 1 cm, the system can be effectively discharged for a longer time, the discharging time decreases from 180 to 114

min in the case of slag pebbles packed-bed system. While in the case of a quartzite rock packed-bed, it decreases from 158 to 112 min. This can be attributed to an increase in the volumetric heat transfer coefficient between the molten-salt and the solid particles as the particle diameter decreases. This leads to a faster process of heat transfer within a storage device.

The time required for the complete discharging process is listed in Table 4.

As evident from Fig. 12, when the particle diameter is small, the discharge performance of slag pebbles packed-bed becomes more and more stable. As particle size is 1 cm in diameter, the energy stored during the charging period is completely extracted during the discharge period. In addition, as the particle diameter increases, the heat exchange zone of the TES system expands further, resulting in an earlier fall in discharging power profiles. This can be attributed to increased thermal gradients of the packed-bed TES system. The stability of the discharge performance for the heat-supply enhances when $D_p = 1$ cm and any changes in D_P above 1 cm have a relative effects on the overall thermal performance of the TES system.

4. Conclusions

A transient two-dimensional model based on local non-equilibrium thermal theory for the porous medium has been developed to investigate the single charging and discharging processes for the molten-salt packed-bed thermocline tank. The influences of various operating parameters, such as the inlet flow rate of charging /discharging and diameter of the solid particles are investigated. All the results obtained are compared to the pure molten-salt tank. The following conclusions are summarized as follows:

(1) A pure molten-salt tank achieves better thermal stratification than a packed-bed tank in a simple charging/discharging process, but the thermal stratification of the packed-bed tank is better at a lower flow rate. In addition, alumina ceramics have a higher thermocline thickness compared to slag pebbles and quartzite rock.
(2) Thermocline thickness for different storage systems increases as the flow rate increases. Slag pebbles packed-bed system achieves a percentage increase in thermocline thickness of about 228% with reference to pure molten-salt tank at a higher flow rate of 0.9 m^3/h, while this percentage decreases to 57.14% when operating at a flow rate of 0.3 m^3/h.
(3) Slag pebbles achieve a longer steady-state outlet temperature period than quartzite rock, hence the discharge performance of the TES system using slag pebbles is more effective than another one used a quartzite rock.
(4) Decreasing the particle size from 4 cm to 1 cm reduces the thermal gradients within a storage device and reduces the time required for complete charging. It also improves the stability of the discharge outlet temperature for the steam generation and consequently enhances the discharge performance.

Declaration of Competing Interest

The authors declare that they have no known competing financial interests or personal relationships that could have appeared to influence the work reported in this paper.

CRediT authorship contribution statement

ELSaeed Saad ELSihy: Investigation, Data curation, Formal analysis, Writing - original draft. **Zhirong Liao:** Investigation, Methodology. **Chao Xu:** Methodology. **Xiaoze Du:** Conceptualization, Methodology, Supervision, Writing - review & editing.

Acknowledgments

The financial supports from the National Natural Science Foundation of China (No. 51676069 and 51821004) are gratefully acknowledged.

References

[1] S.J. Lock, S.T. Stewart, M. Ćuk, The energy budget and figure of Earth during recovery from the Moon-forming giant impact, Earth Planet. Sci. Lett. 530 (2020), doi:10.1016/j.epsl.2019.115885.
[2] T. Sokhansefat, A.B. Kasaeian, F. Kowsary, Heat transfer enhancement in parabolic trough collector tube using Al 2O3/synthetic oil nanofluid, Renew. Sustain. Energy Rev. 33 (2014) 636–644, doi:10.1016/j.rser.2014.02.028.
[3] F.S. Javadi, R. Saidur, M. Kamalisarvestani, Investigating performance improvement of solar collectors by using nanofluids, Renew. Sustain. Energy Rev. 28 (2013) 232–245, doi:10.1016/j.rser.2013.06.053.
[4] M.Y. Abdelsalam, H.M. Teamah, M.F. Lightstone, J.S. Cotton, Hybrid thermal energy storage with phase change materials for solar domestic hot water applications: Direct versus indirect heat exchange systems, Renew. Energy 147 (2020) 77–88, doi:10.1016/j.renene.2019.08.121.
[5] S.S. Mostafavi, M. Saffar-avval, S. Behboodi, Z. Mansoori, Hourly energy analysis and feasibility study of employing a thermocline TES system for an integrated CHP and DH network, Energy Convers. Manag. 68 (2013) 281–292, doi:10.1016/j.enconman.2013.01.020.
[6] L.F. Cabeza, C. Solé, A. Castell, E. Oró, A. Gil, Review of solar thermal storage techniques and associated heat transfer technologies, Proc. IEEE 100 (2) (2012) 525–538, doi:10.1109/JPROC.2011.2157883.
[7] Z. Chang, et al., The effect of the physical boundary conditions on the thermal performance of molten salt thermocline tank, Renew. Energy 96 (2016) 190–202, doi:10.1016/j.renene.2016.04.043.
[8] J.E. Pacheco, S.K. Showalter, W.J. Kolb, Development of a molten-salt thermocline thermal storage system for parabolic trough plants, J. Sol. Energy Eng. Trans. ASME 124 (2) (2002) 153–159, doi:10.1115/1.1464123.
[9] G. Angelini, A. Lucchini, G. Manzolini, Comparison of thermocline molten salt storage performances to commercial two-tank configuration, Energy Procedia 49 (2014) 694–704, doi:10.1016/j.egypro.2014.03.075.
[10] N. Nallusamy, S. Sampath, R. Velraj, Experimental investigation on a combined sensible and latent heat storage system integrated with constant/varying (solar) heat sources, Renew. Energy 32 (7) (2007) 1206–1227, doi:10.1016/j.renene.2006.04.015.
[11] C. Xu, Z. Wang, Y. He, X. Li, F. Bai, Sensitivity analysis of the numerical study on the thermal performance of a packed-bed molten salt thermocline thermal storage system, Appl. Energy 92 (2012) 65–75, doi:10.1016/j.apenergy.2011.11.002.
[12] C. Xu, X. Li, Z. Wang, Y. He, F. Bai, Effects of solid particle properties on the thermal performance of a packed-bed molten-salt thermocline thermal storage system, Appl. Therm. Eng. 57 (1–2) (2013) 69–80, doi:10.1016/j.applthermaleng.2013.03.052.
[13] H. Yin, J. Ding, X. Yang, Experimental research on thermal characteristics of a hybrid thermocline heat storage system, Appl. Therm. Eng. 62 (1) (2014) 293–301, doi:10.1016/j.applthermaleng.2013.09.018.
[14] H. Yin, J. Ding, R. Jiang, X. Yang, Thermocline characteristics of molten-salt thermal energy storage in porous packed-bed tank, Appl. Therm. Eng. 110 (2017) 855–863, doi:10.1016/j.applthermaleng.2016.08.214.
[15] A. Abdulla, K.S. Reddy, Effect of operating parameters on thermal performance of molten salt packed-bed thermocline thermal energy storage system for concentrating solar power plants, Int. J. Therm. Sci. 121 (2017) 30–44, doi:10.1016/j.ijthermalsci.2017.07.004.
[16] A. Bruch, S. Molina, T. Esence, J.F. Fourmigué, R. Couturier, Experimental investigation of cycling behaviour of pilot-scale thermal oil packed-bed thermal storage system, Renew. Energy 103 (2017) 277–285, doi:10.1016/j.renene.2016.11.029.
[17] B. chen Zhao, M. song Cheng, C. Liu, Z. min Dai, Cyclic thermal characterization of a molten-salt packed-bed thermal energy storage for concentrating solar power, Appl. Energy 195 (2017) 761–773, doi:10.1016/j.apenergy.2017.03.110.
[18] M. Cascetta, F. Serra, G. Cau, P. Puddu, Comparison between experimental and numerical results of a packed-bed thermal energy storage system in continuous operation, Energy Procedia 148 (2018) 234–241, doi:10.1016/j.egypro.2018.08.073.
[19] M. Cascetta, G. Cau, P. Puddu, F. Serra, A comparison between CFD simulation and experimental investigation of a packed-bed thermal energy storage system, Appl. Therm. Eng. 98 (2016) 1263–1272, doi:10.1016/j.applthermaleng.2016.01.019.
[20] Z. Yang, S.V. Garimella, Cyclic operation of molten-salt thermal energy storage in thermoclines for solar power plants, Appl. Energy 103 (2013) 256–265, doi:10.1016/j.apenergy.2012.09.043.
[21] M.J. Li, Y. Qiu, M.J. Li, Cyclic thermal performance analysis of a traditional Single-Layered and of a novel Multi-Layered Packed-Bed molten salt Thermocline Tank, Renew. Energy 118 (2018) 565–578, doi:10.1016/j.renene.2017.11.038.
[22] Z. He, Y. Qian, C. Xu, L. Yang, X. Du, Static and dynamic thermocline evolution in the water thermocline storage tank, Energy Procedia 158 (2018) (2019) 4471–4476, doi:10.1016/j.egypro.2019.01.766.

[23] Z. He, X. Wang, X. Du, M. Amjad, L. Yang, C. Xu, Experiments on comparative performance of water thermocline storage tank with and without encapsulated paraffin wax packed bed, Appl. Therm. Eng. (2018), doi:10.1016/j.applthermaleng.2018.10.051.
[24] Z. He, X. Wang, X. Du, C. Xu, L. Yang, Cyclic characteristics of water thermocline storage tank with encapsulated PCM packed bed, Int. J. Heat Mass Transf. 139 (2019) 1077–1086, doi:10.1016/j.ijheatmasstransfer.2019.05.093.
[25] S. Wu, G. Fang, X. Liu, Dynamic discharging characteristics simulation on solar heat storage system with spherical capsules using paraffin as heat storage material, Renew. Energy 36 (4) (2011) 1190–1195, doi:10.1016/j.renene.2010.10.012.
[26] X. Du, Z. He, X. Wang, C. Xu, L. Yang, Unsteady characteristics of water thermocline storage tank with encapsulated paraffin wax packed bed, Int. Heat Transf. Conf. 2018-Augus (2018) 4287–4294, doi:10.1615/ihtc16.ecs.022477.
[27] K. Nithyanandam, R. Pitchumani, A. Mathur, Analysis of a latent thermocline storage system with encapsulated phase change materials for concentrating solar power, Appl. Energy 113 (2014) 1446–1460, doi:10.1016/j.apenergy.2013.08.053.
[28] K.E. Elfeky, N. Ahmed, Q. Wang, Numerical comparison between single PCM and multi-stage PCM based high temperature thermal energy storage for CSP tower plants, Appl. Therm. Eng. 139 (February) (2018) 609–622, doi:10.1016/j.applthermaleng.2018.04.122.
[29] J.F. Hoffmann, T. Fasquelle, V. Goetz, X. Py, A thermocline thermal energy storage system with filler materials for concentrated solar power plants: Experimental data and numerical model sensitivity to different experimental tank scales, Appl. Therm. Eng. 100 (2016) 753–761, doi:10.1016/j.applthermaleng.2016.01.110.
[30] A. Mawire, M. McPherson, Experimental characterisation of a thermal energy storage system using temperature and power controlled charging, Renew. Energy 33 (4) (2008) 682–693, doi:10.1016/j.renene.2007.04.021.
[31] B. Xu, P. Li, C.L. Chan, Energy Storage Start-up Strategies for Concentrated Solar Power Plants With a Dual-Media Thermal Storage System, J. Sol. Energy Eng. Trans. ASME 137 (5) (2015) 1–12, doi:10.1115/1.4030851.
[32] P.A. Galione, C.D. Pérez-Segarra, I. Rodríguez, A. Oliva, J. Rigola, Multi-layered solid-PCM thermocline thermal storage concept for CSP plants. Numerical analysis and perspectives, Appl. Energy 142 (2015) 337–351, doi:10.1016/j.apenergy.2014.12.084.
[33] S. Shiri, "A Model of Transient Heat Transfer in a Packed Bed of Alumina Particles," *MSc thesis, City Univ. New York*, 2013.
[34] T. D. Canonsburg, "ANSYS Fluent Tutorial Guide," vol. 15317, no. November, pp. 724–746, 2013.
[35] K. s, F.T. Wakao N, Effect of fluid dispersion coefficients on particle-to-fluid heat transfer coefficients in packed beds, Chem. Eng. Sci. 34 (1–2) (1979) 325–336.
[36] R. Ferri, A. Cammi, D. Mazzei, Molten salt mixture properties in RELAP5 code for thermodynamic solar applications, Int. J. Therm. Sci. 47 (12) (2008) 1676–1687, doi:10.1016/j.ijthermalsci.2008.01.007.
[37] F. Cabello Núñez, J. López Sanz, F. Zaversky, Analysis of steel making slag pebbles as filler material for thermocline tanks in a hybrid thermal energy storage system, Sol. Energy 188 (February) (2019) 1221–1231, doi:10.1016/j.solener.2019.07.036.